OBSERVATION OF TURBULENCE CHARACTERISTICS IN THE ŌTA RIVER USING ADV AND HRCP

Mahdi Razaz [1], Prof. Kiyosi Kawanisi[2]

[1]Member of JSCE, M. Eng., River and Coastal Engineering Laboratory, Dept. of Civil & Environmental Engineering, Hiroshima University (1-4-1, Kagamiyama, Higashi-Hiroshima 739-8527, Japan)
[2]Member of JSCE, Dr. of Eng., Associate Professor, Dept. of Civil & Environmental Engineering, Hiroshima University (1-4-1, Kagamiyama, Higashi-Hiroshima 739-8527, Japan).

Acoustic Doppler Current Profilers (ADCP) and Velocimeters (ADV) have been increasingly used for measuring small-scale processes involving turbulence in estuarine environments. A point at the center of the Ōta Floodway, 2.8 km far from mouth, was selected to deploy an ADV and a HRCP (High-Resolution ADCP) during 25 hours of Jan. 2009. Obtained data were despiked and analyzed in order to first examine turbulence parameters calculated from HRCP data. Next, estimate TKE production and dissipation rates from 1D spectra of vertical component of velocity *w* and using Kolmogorv's -5/3 power law. Then, redefine M-Y model parameters of proportionality constant B_1 and stability function S_M. Finally, inter-compare HRCP and ADV in 3 reference levels of 0.03, 0.4, and 0.8 mab along with *w*-spectra and turbulence energy spectra reveal that *w'* is underestimated by HRCP which leads to lower dissipation rates comparing to ADV. Also, longitudinal velocity fluctuations *u'* of ADV are underestimated, as a result streamwise Reynolds stress of ADV is less than that obtained from HRCP at bottom level.

Key Words: *Acoustic Doppler effect, estuaries, tidal currents, turbulence, M-Y model, power spectrum*

1. INTRODUCTION

To overcome the complexity caused by dynamic natural elements e.g. tidal oscillation, river discharge, wind driven waves, etc. instruments referred to as pulse-to-pulse coherent Doppler sonar have been developed. These instruments are able of collecting data *in situ* with high quality throughout water column and observation period. Backscattered data can be translated into velocity components, suspended sediment concentration (SSC), sound speed in water, etc. These instruments have been widely used by scientists to conduct various measurements in complex flow fields, e.g. Hill *et al.*[1], Fugate and Friedrichs[2], Muste *et al.*[3], and Kawanisi[4].

Drawbacks of using instruments based on acoustic pulse-to-pulse coherent sonar can be divided into 2 main groups: a) intrinsic: issues in converting raw backscattered wave data to figures/numbers inside the instrument (e.g. Lohrmann and Nylund[5]); b) extrinsic: ambiguities in rendering raw collected data into applicable knowledge such as SSC. At the present paper, by processing backscatter data and applying necessary corrections (*e.g.* Downing *et al.*[6]; Thorne *et al.*[7]; Hill *et al.*[1]), raw backscatter data translated into vertical profiles of velocity and SSC. HRCP analyzed data will be reviewed and compared to the data acquired by an ADV to focus on the latter problem with intercomparing HRCP and ADV. According to Voulgaris and Throwbridge[8] ADV data are precise.

2. STUDY AREA AND OBSERVATION METHOD

Ōta Floodway is the most-west branch of the Ōta River with a length of nearly 9 km. It is a tidally-dominated river and the maximum tidal range in an extreme spring tide can reach 4 m close to the mouth (**Fig. 1**). Fresh water inflow to the Ōta Floodway is controlled by the Gion sluice gates that are located in the bifurcation place. The Gion sluice gates consist of 3 main gates that generally just one of them is opened to provide a 32×0.3 m^2 cross section for spilling the flow into the Ōta Floodway. From this cross section about 10% of flow in the main branch of the Ōta River is diverted to the floodway in normal days. However during the flood event, the Gion sluice gates are opened as to divert 50% of total fresh water to the floodway.

In our observations we operated a commercially-available HRCP: HR-AquaDopp and an ADV: Vectrino$^+$, both developed by NORTEK AS Co.

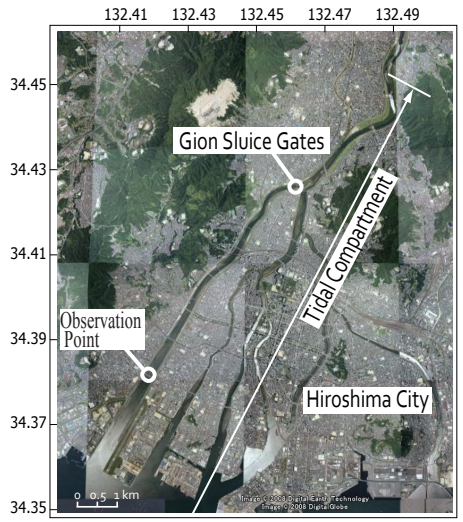

Fig. 1 Map of the observation point.

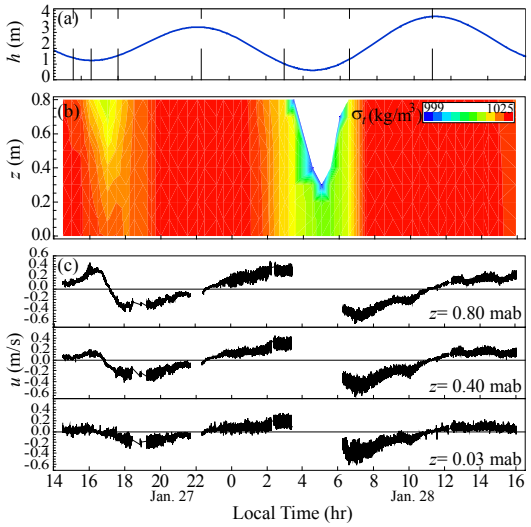

Fig. 2 Temporal variations of (a) water depth, (b) density (σ_t) profile, and (c) instantaneous longitudinal velocity u.

However mean velocity collected by the ADV and ADCP are assumed to be identical (Stone and Hotchkiss[9]), there are uncertainties about fluctuating part of measured velocity by ADCPs mainly because of low time resolution, their relatively large sampling volumes, and using 3 or 4 separated beams that move away from each other as the beam length increases. In order to measure velocity profile precisely, the HRCP was installed down-looking as the transducers were 1 m above the bed (mab). To prevent device from being shaken by currents it was fixed on a special frame. Data was collected at 1.0 Hz sampling rate and 2.0 cm cell depth. Blanking distance was set to 5 cm. To measure the turbulence just near to the bed we deployed the ADV with a synchronized compass/tilt in about 8 cm far from the bed that its beams intersect in approximately 50 mm far from the center of sampling volume. Every 20 minutes location of the ADV was changed so as to measure velocity components in 0.03, 0.40, and 0.80 mab. A Conductivity/Temperature/Depth (CTD) probe developed by Alec Electronics Co. was casted every 30 minutes to check salinity and density profiles in 10 cm depth-triggered mode. The observation fulfilled over 25 hours of 27-28 Jan. 2009 using described instruments in a point that is located 2.8 km far from the river mouth at the center of the river (**Fig. 1**). Water depth, salinity and velocity variations in observation time-span are shown in **Fig. 2**.

3. DEPTH-TIME VARIATION OF TURBULENCE

Depth-time variation of turbulence parameters averaged over 5-minute intervals estimated from HRCP data are shown in **Fig. 3**. Areas with absolute white color denote the omitted erroneous data mainly near the upper and lower edges. These erroneous areas may be a correspondence to the sign reversal of the streamwise Reynolds shear stress $-\overline{u'w'}$ around the end of ebb, a consequence of unreliable stress estimations, or HRCP limitations in highly stratified flow. The gray stripe indicates the lower low water in which HRCP transducers were dried out. In **Fig. 3(a)** variations of the longitudinal Reynolds shear stress $-\overline{u'w'}$ in depth is plotted. Hereafter symbols ↑ and ↓ stands for approximate HWS and LWS time in figures, respectively. Over the observation period $|\overline{u'w'}|$ is relatively low. According to **Fig. 3(a)**, this variable reaches its peak values just before and after lower low water slack (LWS). Referring to **Fig. 2(c)** reveals that longitudinal Reynolds stress and velocity

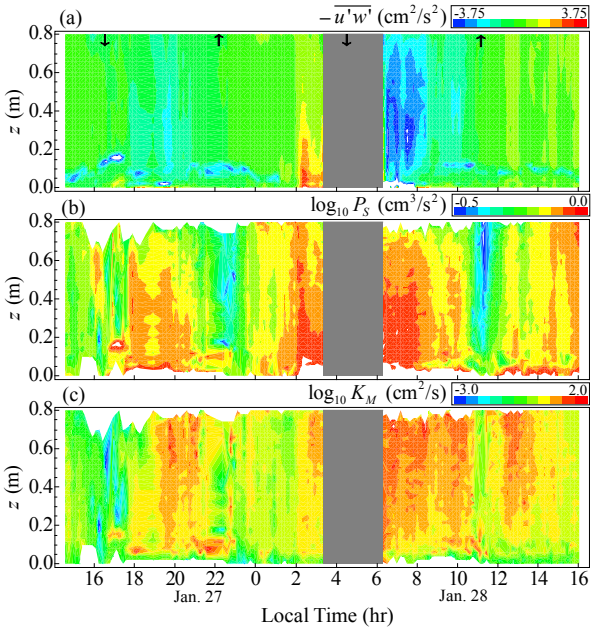

Fig. 3 Depth-time distributions of (a) Reynolds stress, (b) shear production, and (c) eddy viscosity.

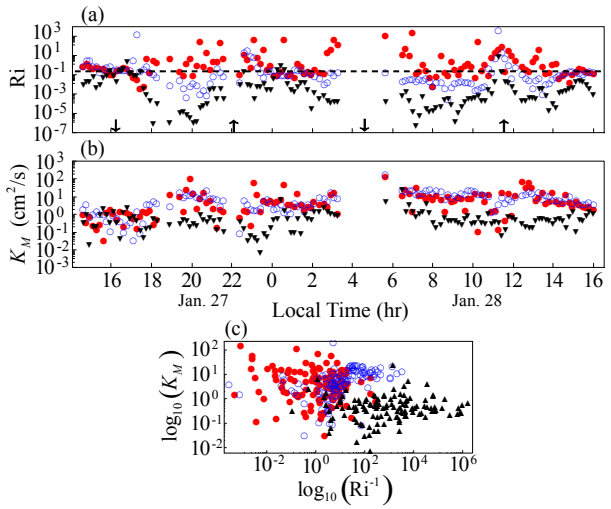

Fig. 4 Temporal variations of (a) local gradient Richardson number, (b) vertical eddy viscosity and (c) scatter plot of K_M variations as a function of Ri^{-1} in 0.8 (●), 0.4 (○), and 0.03 mab (▼).

component u are in phase. Since TKE shear production P_s is a function of Reynolds stress, it is expected to find the highest magnitudes of P_s at the same time as Reynolds stress (**Fig. 3(b)**). **Fig. 3(c)** exhibits spatiotemporal variations of eddy viscosity coefficient K_M that is a function of P_s and means velocity gradients; hence it is in proportion with P_s and or $-\overline{u'w'}$. Magnitudes of K_M in the second tide were generally higher than those in the first tide; especially, after the lower LWS all over the flood duration K_M was high. During the first ebb and particularly in LWS, K_M had very small values near the bottom, corresponding to weak near-bed-generated turbulence.

Stratification of the river bottom layer is taken into account by plotting Richardson number Ri obtained from the HRCP data. In **Fig. 4(a)** dash line denotes the critical value of ¼. Ri in the near-bottom layer rarely exceeds ¼ and in floods lowest Richardson numbers are noticeable, while large values of Ri could be found in the upper layer in slack waters particularly in HWS. **Fig. 4(c)** suggests that K_M and Ri^{-1} are in good agreement.

Rates of TKE production and dissipation are plotted in **Figs** 5 and **6**. Selected sections are marked by dash lines in **Fig. 2(a)**. We used Kolmogorov's -5/3 power law to describe 1D kinetic energy density as a function of energy dissipation ε. Buoyant production P_b is estimated assuming K_M=K_H, where K_H is the vertical eddy diffusivity. As it is expected to observe larger magnitudes of shear production P_s before and after of LWS, uppermost values of shear production are discernible in the second LWS near the bed and in the following flood with around 0.4 and 1 cm^2/s^3, respectively (**Fig. 6**). Although during the first tide buoyant production rate P_b is insignificant, in the following ebb and flood in about 0.7 mab outstanding magnitudes of this variable can be seen. Since rate of energy dissipation is often less than P_b+P_s except in the HWS according to the HRCP data set, we cannot assume a continuous local balance between TKE production and dissipation. In order to confirm the method and hardware applied to obtain TKE production and dissipation rates, we conducted short-term measurements in a laboratory flume using the same HRCP. Results notify an acceptable compliance between kinetic energy production and dissipation. This imbalance is reported by Kawanisi[4] and confirmed in our previous study at the same point (Razaz *et al.*[10]). Such an imbalance that was studied by Satcey *et al.*[11]) may stem from unsteady state of flow during tidal phases or underestimation of w' by HRCP (**Fig. 15**).

Vertical eddy viscosity K_M as a function of ql_m at 0.03, 0.4 and 0.8 mab for the ebb and flood phase is plotted in **Fig. 7**. q is the turbulence energy and l_m refers to the mixing length. Apparently K_M and ql_m are in good proportion, and if we accept that turbulent mixing length in M-Y model l is equal to l_m, ratio of K_M/ql_m represents the amount of M-Y stability function S_M. From proportionalities shown in **Fig. 7** it is inferred that during flood S_M≈0.22 which is slightly greater than that in the ebb. Kawanisi[4] calculated the highest value of S_M=0.29 during flood. In our previous observation S_M calculated as 0.25. All these signify that S_M in M-Y model which is calculated under neutral condition, is not valid here because under unstratified equilibrium conditions Gulperin *et al.*[12] function gives S_M=0.39, while highest S_M in flood, when stratification is negligible, is less than 0.3.

Fig. 8 is the scatter diagram of dissipation ε against q^3/l_m. In M-Y model B_1=16.6, though here B_1 is outstandingly larger, particularly near the bed. Very small dissipation rates obtained from the

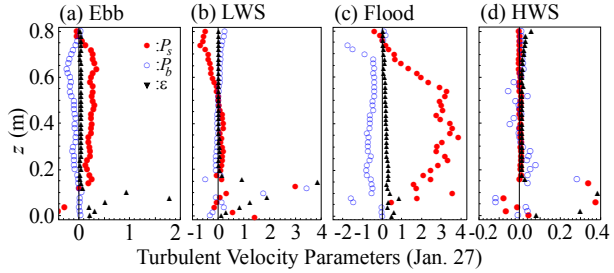

Fig. 5 Typical profiles of turbulence energy production and dissipation rate: 10P_s (○), 10P_b (●), and 10ε (▲).

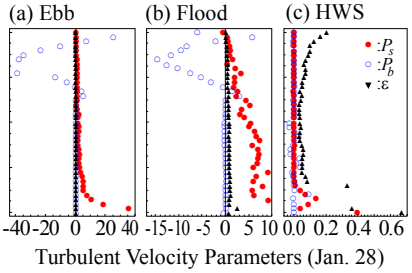

Fig. 6 Typical profiles of turbulence energy production and dissipation rate: 10P_s (○), 10P_b (●), and 10ε (▲).

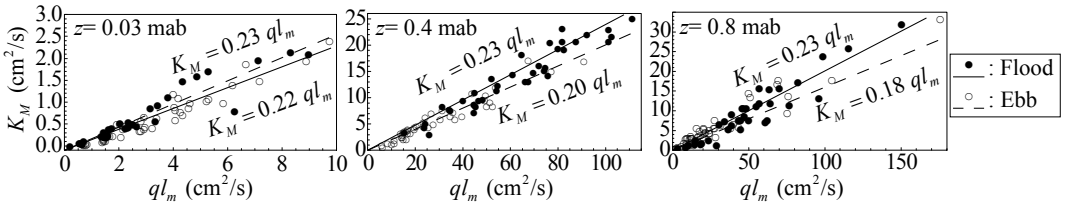

Fig. 7 Relation between ql_m and K_M in different levels and tidal phases.

HRCP data are responsible for these extraordinary high values. If we accept $\varepsilon=P_b+P_s$, then B_1 could be roughly estimated as 70 by replacing ε with P_b+P_s in **Fig. 9**. According to this figure and the way B_1 is calculated, it is proposed that ε is underestimated from HRCP data by an order of 10, averagely. Kawanisi[4] calculated this constant about 40 assuming $\varepsilon=P_s$. Also, we already calculated this constant about 40 assuming $\varepsilon=P_s$. Also, we already calculated this constant as 55 under the same assumption. These results recommend a higher value for B_1 instead of the original value.

4. INTERCOMPARING PERFORMANCE OF HRCP AND ADV

(1) Turbulence parameters

In this section we will try to compare key turbulence parameters at 3 reference levels of 0.03, 0.4 and 0.8 mab obtained from analyzing raw data collected by the ADV and HRCP. In the following figures, $U=(u^2+v^2)^{1/2}$; u, v, and w are longitudinal, transverse, and vertical components of velocity, respectively; prime sign denotes variation from the mean value; and "–" stands for averaging over time. Absolute values of longitudinal and vertical velocity fluctuations can be defined as $\sigma_u=\left(\overline{u'^2}\right)^{1/2}$, $\sigma_w=\left(\overline{w'^2}\right)^{1/2}$, respectively.

Values of plotted variables according to Mellor and Yamada[13] in a neutral equilibrium boundary layer are defined as: $\sigma_u/u_*\approx 2$, $\sigma_w/\sigma_u\approx 0.5$, and $|\overline{u'w'}|/q^2\approx 0.15$. On the other hand, Nezu and Nakagawa[14] showed that $|\overline{u'w'}|/q^2$ varies between 0.1 near the bed, reaches 0.04 near the water surface, and in the middle of water column is 0.15. **Fig. 10** shows temporal variations of the streamwise Reynolds stress RS over the observation period. Best convergence between HRCP and ADV data can be recognized near the bed, where $RS_{ADV}= 0.83\ RS_{HRCP}$ over the observation length. In 0.4 mab, difference between measurements of the two sensors increases to its maximal, while in 0.8 mab we can observe less disparity. This pattern can be observed in other turbulence statistics variations. In **Fig. 11** ratio of σ_u/u_*, u_* is the shear velocity, is plotted. Mean near-bed value for ADV is around 3 and rises to 7 for HRCP data.

Considering **Fig. 12** reveals that value of σ_w/σ_u didn't change noticeably with distance from bed for both sensors. Mean values of this ratio for the ADV data is about 0.48 and for the HRCP estimated as 0.28 for each of three reference levels. Concerning Figs. 10, 11, and 12 it can be inferred that σ_u and σ_w are underestimated by ADV and HRCP, respectively. Also, inspecting u-spectra of ADV data reveals that they are saturated at 0.2 Hz. This frequency is too high under field scale considerations.

Variations of ratio of longitudinal Reynolds stress to the turbulence energy are plotted in **Fig. 13**. Mean values of this parameter doesn't show remarkable changes related to depth. In general, estimations from ADV data are 70% larger than that from HRCP. Finding largest magnitudes in slack waters, suggests that inactive and effectively irrotational part of turbulence is larger as cited in Bradshaw[15]. Inactive part of turbulence doesn't produce any shear stress and is determined by the turbulence in the outer layer. This inactive motion is generated as a result of density interface in water column that acts like a free surface and suppresses the vertical movement of eddies. Mean value of ADV data set is about 0.08, while for the HRCP data set is half of that. Assuming $l= l_m$, it is inferred that $|\overline{u'w'}|/q^2=S_M^2$. According to Stacey *et al.*[11] equivalency of l and l_m in stratified turbulent boundary layer is acceptable. From this method, averaged values of S_M over the observed period are

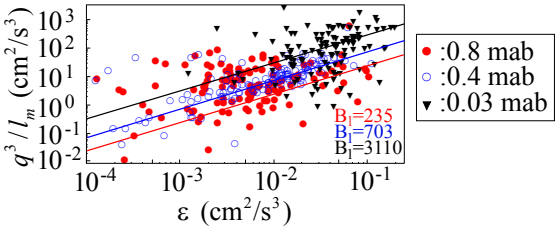

Fig. 8 Scatter diagram of energy dissipation rate against q^3/l_m.

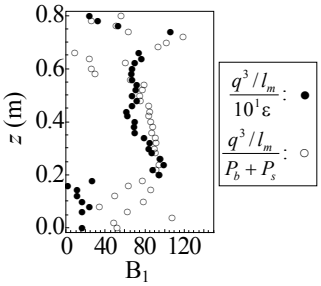

Fig. 9 Vertical profile of constant B_1.

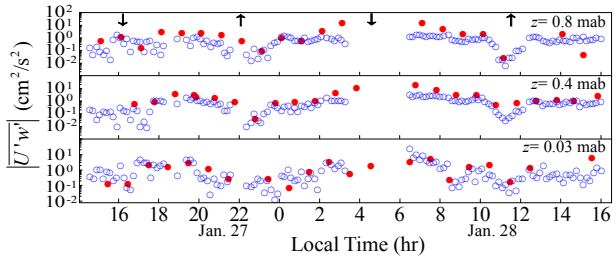

Fig. 10 Comparison between streamwise Reynolds stresses acquired from HRCP data (○) and ADV data (●).

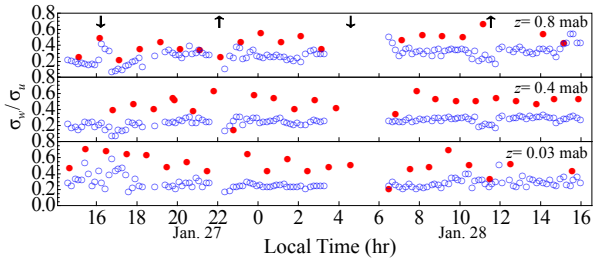

Fig. 12 Comparison between evaluated σ_w/σ_u acquired from HRCP data (○) and ADV data (●).

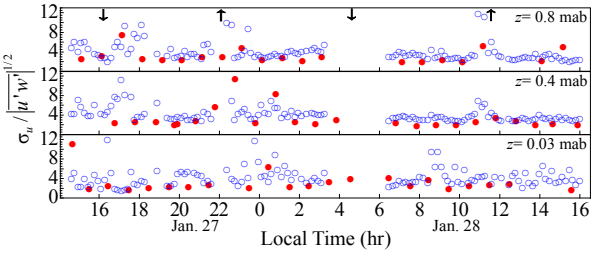

Fig. 11 Comparison between evaluated $\sigma_u/|\overline{u'w'}|^{1/2}$ acquired from HRCP data (○) and ADV data (●).

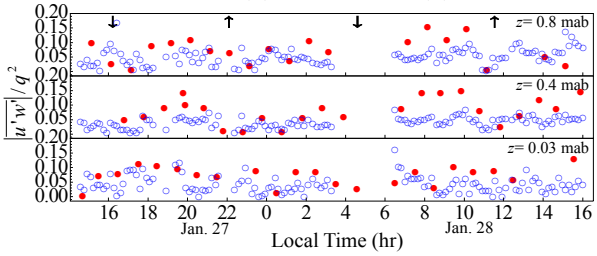

Fig. 13 Comparison between evaluated $|\overline{u'w'}|/q^2$ acquired from HRCP data (○) and ADV data (●).

approximately 0.2 and 0.28 using HRCP and ADV data, respectively.

(2) Spectral Characteristics

(Power) Spectral density functions or simply the (power) spectra of turbulence energy q^2 as measured by the ADV and HRCP sensors are examined here. The spectra from whole observation time span in 3 reference levels are presented in **Fig. 14**, in which f represents the sampling rate of each sensor. These spectra are computed by Fast-Fourier Transform (FFT) method (He[16]). Evidently, both sensors have the same energy level except in near-bed level. While the ADV waves carry no energy in frequencies less than 5×10^{-1} Hz, this limit is extended to 5×10^{-2} Hz for the HRCP. It is unknown to us why the energy of ADV spectrum dropped down in 0.03 mab. As another comparison between the HRCP and ADV we examine the 1D spectra of vertical component of velocity w. In particular the spectra represented in **Fig. 15** belong to flood phase when velocity fluctuations are remarkable. These spectra illustrate that ADV turbulence velocity spectra contain more energy than that of HRCP. HRCP w-component contains quite less fluctuations rather than ADV data. In addition, mean value of w_{HRCP} is smaller than that of ADV at the same intervals. This problem intensifies with distance from bed. For both sensors there is no sudden change in the slope indicating that the noise floor is approached. Spectra of both ADV and HRCP decay at relatively high f values with a -5/3 rolloff all the way up to half of sampling frequency.

(3) Dissipation

In this part, dissipation calculated from 1D spectra of w-component will be discussed. As shown in **Fig. 16**, HRCP dissipation rate is less than production rate except in short times. ADV dissipation rate in 0.03 mab is smaller than in 0.8 mab, however it seems to be overestimated in 0.4 mab. The larger values of dissipation and turbulence statistics in 0.4 mab can be a consequence of boundary effects. In spite of setting nominal velocity of ADV to 0.1, 0.3 or 1 m/s which are attributed to weak spots at 46; 20; 8, 20 cm far from boundary, respectively, it seems that boundary effect is yet considerable in 0.4 mab. ε_{HRCP} is smaller than ε_{ADV} as a result of lower energy range of w-spectra at the same frequency span. Unfortunately, we cannot estimate P_s from ADV data accurately, since number of observed points in the water column is not enough to produce a reliable velocity distribution. However, laboratory tests conducted in a flume using the same HRCP resulted in equivalence of dissipation and production of TKE. Hence, we may assume that turbulent nature of flow in tidal rivers causes some disabilities in the HRCP.

4. CONCLUSION

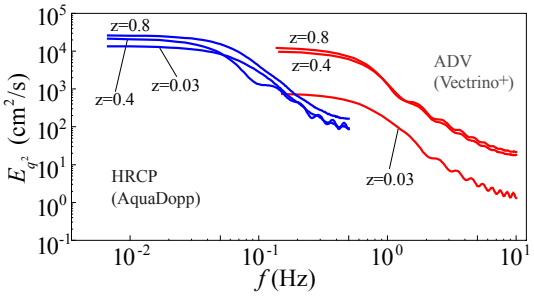

Fig. 14 Power spectrum of turbulence energy computed from HRCP and ADV data at 3 reference levels.

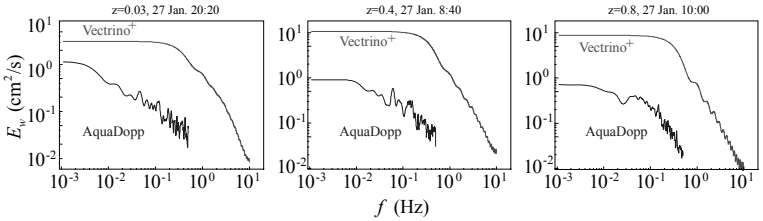

Fig. 15 Power spectra of w-component in 3 different level and tidal phase.

Examining spatiotemporal variations of longitudinal Reynolds shear stress reveals that just before and after lower LWS this variable increases to its absolute peak values. However in flood time Reynolds stress stays in relatively high levels. Subsequently, TKE production rate and vertical eddy viscosity that are a function of Reynolds stress are augmented at the same time as Reynolds stress. Because other factors such as velocity gradients and turbulent mixing length affect the latter two variables, their spatiotemporal variations don't exactly follow Reynolds stress fluctuations. During HWS/LWS flow becomes highly stratified especially in upper layers. Maximum stability function found to be 0.23 which is quite less that Gulperin's function[12] result in unstratified equilibrium conditions. This means the assumption of neutral conditions in M-Y model for estimating stability function is invalid. According to the HRCP result, TKE production and dissipation rates are not equal except in HWS that P_s is in its lowest rates. It seems that dissipation is underestimated by an order of 10 from the HRCP data that leads to outstanding magnitude of B_1. Comparing turbulence statistics together with *u*- and *w*-spectra reveals that *u'* and *w'* are underestimated by ADV and HRCP, respectively. Streamwise Reynolds stress of ADV, except at bottom level, is larger than that of HRCP. As a result, σ_w/σ_u and σ_u/u_* measurements are divergent for both instruments. However, S_M values of both sensors are in good agreement.

Finally, plotting spectra of turbulence energy

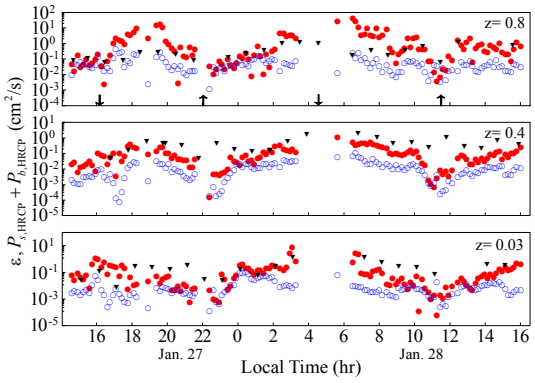

Fig. 16 Temporal variations of TKE production obtained from HRCP data (●) and dissipation rate estimated from HRCP (○) and ADV data (▼).

and *w*-component reveals the difference between energy density of ADV and the HRCP. Lower energy of HRCP *w*-component spectra can explain the underestimation of Reynolds stress and dissipation rates.

More studies could help to reveal more precise differences between these two sensors.

REFERENCES

1) Hill D. C., Jones S. E., and Prandle D.: Derivation of sediment resuspension rates from acoustic backscatter time-series in tidal waters, *J. Continental Shelf Research*, Vol.23, pp. 19-40, 2003.
2) Fugate D. C., and Friedrichs C. T.: Controls on suspended aggregate size in partially mixed estuaries, *J. of Estuarine, Coastal and Shelf Science*, Vol.58, pp. 389-404, 2003.
3) Muste M., Yu K., Pratt T., and Abraham D.: Practical aspects of ADCP data use for quantification of mean river flow characteristics; Part II: fixed-vessel measurements, *J. fluid Measurements and Instrumentation*, pp. 17-28, 2004.
4) Kawanisi K.: Structure of turbulent flow in a shallow tidal estuary, *J. Hydraulic Engineering*, ASCE, Vol.130(4), pp. 360-370, 2004.
5) Lohrmann A., and Nylund S.: Pure coherent Doppler systems - how far can we push it?, Current Measurement Technology, 2008. CMTC 2008. IEEE/OES 9th Working Conference on Current Measurement Technology, Vol.17(19), pp:19 – 24a, 2008.
6) Downing A, Thorne P D and Vincent C E, : Backscattering from a suspension in the near field of a piston transducer, *J. Acoustic Society of America*, Vol.98, pp. 7-16, 1994.
7) Thorne P. D., and Hanes D. M.,: A review of acoustic measurement of small-scale sediment processes, *J. Continental Shelf Research*, Vol.22, pp. 603-632, 2002.
8) Voulgaris, G., and Throwbridge J.H.: Evaluation of the acoustic Doppler velocimeter (ADV) for turbulence measurements, *J. of Atmospheric and Oceanic Technology*, Vol. 5, pp.272-289, 1998.
9) Stone, M. C., and Hotchkiss R. H.: Evaluating velocity measurement techniques in shallow streams", *J. Hydraulic Research*, Vol.45(6), pp.752–762, 2007.
10) Razaz M., Kawanisi K., Yokoyama T.: Turbulent flow in bottom layer of the Ohta River, *Ann.l J. Hydraulic Engg*, JSCE, Vol.53, pp. 193-198, 2009.
11) Satcey M. T., Monismith S. G., and Burau J. R.: Observation of turbulence in a partially stratified estuary, *J. Physical Oceanography*, Vol.129, pp. 1950-1970, 1999.
12) Gulperin B., Kantha L., Hassid S., and Rosati A.: A quasi-equilibrium turbulent energy model for geophysical flows, *J. Atmospheric Science*, Vol.45(1), pp. 55-62, 1988.
13) Mellor G. L., and Yamada T.: Development of a turbulence closure model for geophysical fluid problems, Rev., *J. Geophysical Research-Space Physics*, Vol.20(4): pp. 851-875, 1982.
14) Nezu I., and Nakagawa H.: Turbulence in open-channel flows, Balkema, Rotterdam, The Netherlands, pp. 281, 1987.
15) Bradshaw P: Inactive motion and pressure fluctuations in turbulent boundary layers, *J. Fluid Mechanics*, Vol.30, pp. 241-258, 1967.
16) He Y.: Time series pack; Reference and user's guide, 1st edn, Wolfram Research Inc., Illinois, USA, 1995.

(Received September 30, 2010)